Supplemental material

Wang et al., https://doi.org/10.1083/jcb.201804165

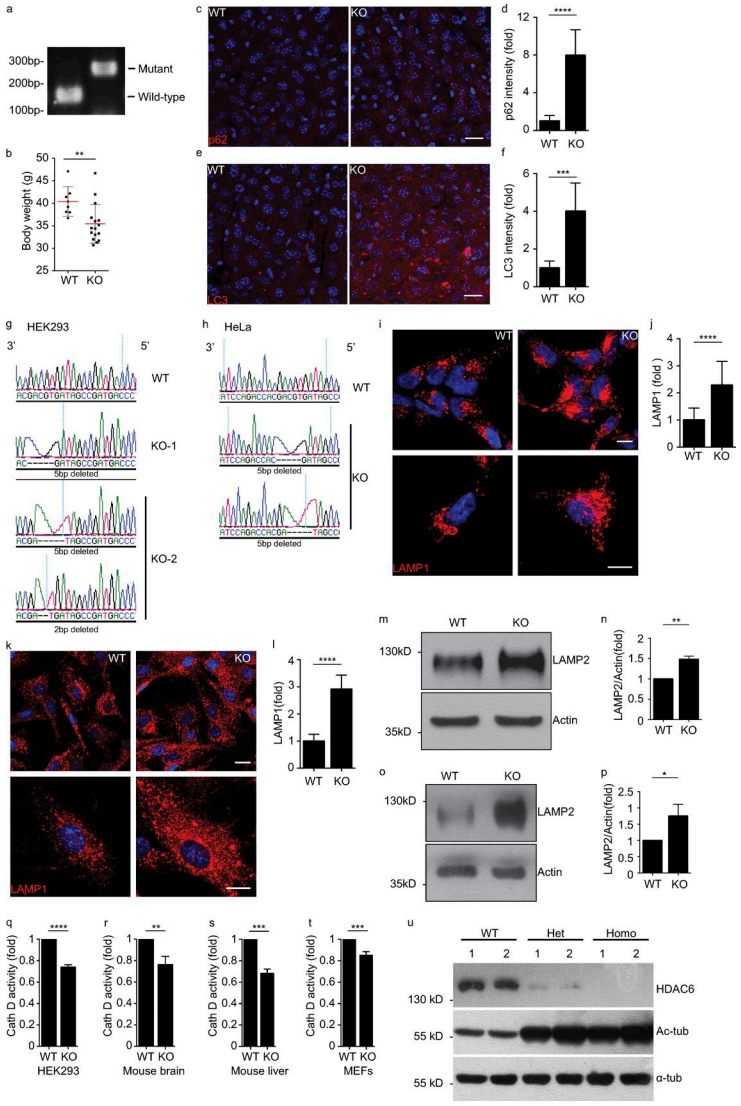

Figure S1. **Characterization of the ATP13A2-deficient mouse line and ATP13A2-deficient cell lines. (a)** Genotyping of ATP13A2-null mouse. Genomic DNAs isolated from tails of WT control mouse (left) and ATP13A2-null mouse (right) were PCR amplified with specific genotyping primers. WT allele products **(**165 bp) and mutant allele products (284 bp) are indicated. **(b)** Decreased body weight of ATP13A2-null mice. Body weights of ATP13A2-null mice (KO) and their control WT littermates at the age of 16–18 mo were measured. **, P < 0.01. WT: *n* = 8, KO: *n* = 16. **(c and d)** p62 expression in mouse livers. Liver sections from ATP13A2-null mice (KO) and their control WT littermates at the age of 16–18 mo were immunostained with an anti-p62 antibody (red). Cell nuclei were counterstained with DAPI (c). The intensity of p62 puncta is quantitated using ImageJ (d). Bar, 20 µm. ****, P < 0.0001. WT: *n* = 19, KO: *n* = 23. **(e and f)** LC3 expression in mouse livers. Liver sections from ATP13A2-null mice (KO) and their control WT littermates (WT) at the age of 16–18 mo were immunostained with an anti-LC3B antibody (red). Cell nuclei were counterstained with DAPI (e). The intensity of LC3 puncta was quantitated with ImageJ (f). Bar, 20 µm, ***, P < 0.001. WT: *n* = 13, KO: *n* = 19. **(g and h)** Characterization of ATP13A2-null HEK293 and HeLa cells. ATP13A2-null HEK293 and HeLa cells were generated with the CRISPR-Cas9 system. Shown are representative sequencing results of ATP13A2-null clones. Note that the ATP13A2-null HEK293 cell KO-1 line carries a 5-bp homozygous deletion, whereas the KO-2 line carries compound heterozygous deletions of 5 bp and 2 bp. As the control, the sequence of WT ATP13A2 in HEK293 cells at targeting sites is shown (g). The ATP13A2-null HeLa cell line harbors two independent compound heterozygous deletions of 5 bp (KO). The sequence of corresponding regions of WT ATP13A2 in HeLa is shown as control (h). **(i and j)** LYS accumulation in ATP13A2-null HEK293 cells. LYS in ATP13A2-null (KO) and WT control cells was immunodetected with an anti-LAMP1 antibody (red). Cell nuclei were counterstained with DAPI (blue). Magnified images are shown in lower panels (i). Quantification of LAMP1-positive structures is shown (j; *n* = 154). Bar, 10 µm. ****, P < 0.0001. **(k and l)** LYS accumulation in ATP13A2-null MEFs. LYS in ATP13A2-null (KO) and WT control cells was immunodetected with an anti-LAMP1 antibody (red). Cell nuclei were counterstained with DAPI (blue). Magnified images are shown in lower panels (k). Quantification of LAMP1-positive structures is shown (l). Bar, 7.5 µm. ****, P < 0.0001, *n* = 100. **(m–p)** Detection of LAMP2 expression in ATP13A2-null cells. Cell lysates of ATP13A2-null (KO) HEK293 cells (m and n), MEFs (o and p) and their matched controls (WT) were immunoblotted with an anti-LAMP2 antibody (m and o). Actin was detected to serve as a loading control. Quantitative analysis of intensity of LAMP2 in HEK293 and MEFs is shown (n and p, respectively; *n* = 3). *, P < 0.05; **, P < 0.01. **(q–t)** Cathepsin D (Cath D) activity in ATP13A2-null HEK293 cells, mouse tissues, and MEF cells. Quantification of Cath D activity in KO ATP13A2-null HEK293 cells (q), and KO mouse brain and liver tissues (r, s), and KO MEF cells (t) and their matched WT control cells. **, P < 0.01; ***, P < 0.001; ****, P < 0.0001, *n* = 3. **(u)** Characterization of HDAC6-null HEK293 cells. HDAC6-null HEK293 cells was generated by using the CRISPR-Cas9 system. Cell lysates of two WT (WT-1, WT-2) clones, two heterozygous (Het-1, Het-2), and two homozygous (Homo-1, Homo-2) HDAC6 mutant clones were analyzed by immunoblotting using antibodies against either HDAC6 or acetyl α-tubulin (Ac-tub). α-Tubulin (α-tub) was detected to serve as a loading control.

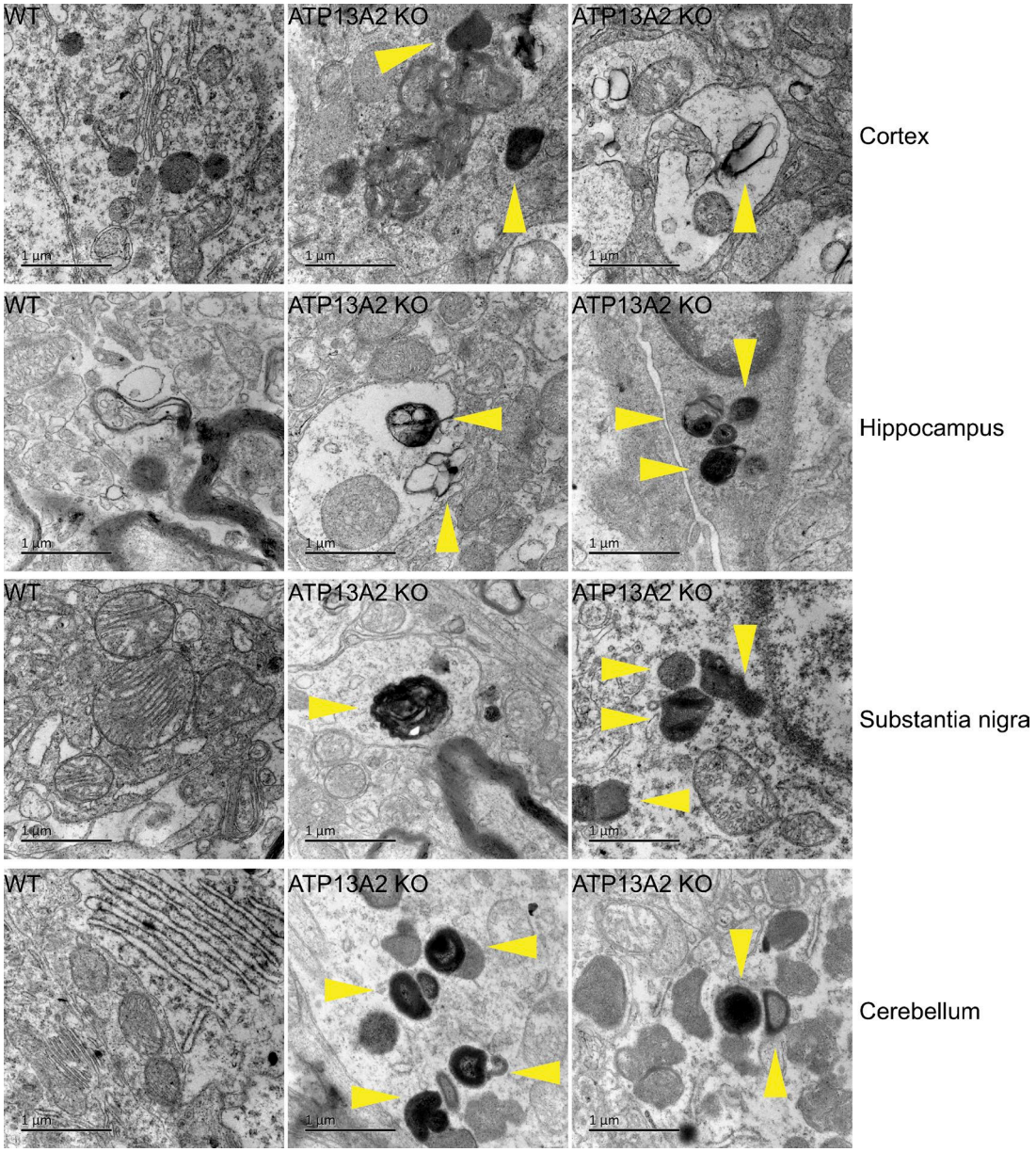

Figure S2. **TEM analysis of ATP13A2-null mouse brain tissues.** Brain tissues from ATP13A2-null (ATP13A2 KO) and their control WT littermates were examined using TEM. Accumulation of abnormal LYS with high electronic density were detected in ATP13A2-null mouse brain tissues, but not in their control WT mouse brain tissues (yellow arrow). Mouse cortex, hippocampus, substantia nigra, and cerebellum were examined. Bar, 1 µm.

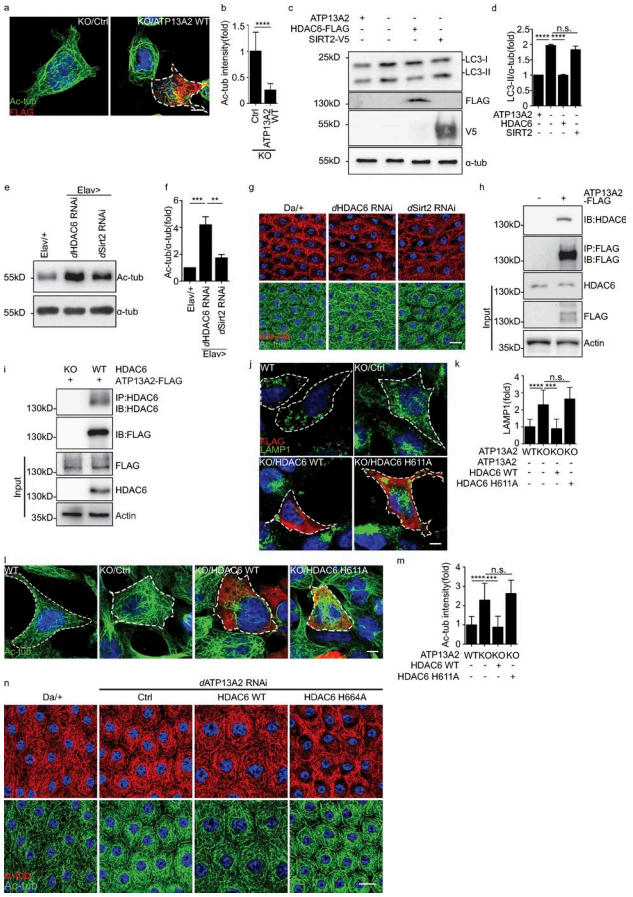

Figure S3. **HDAC6 is a major deacetylase for α-tubulin in both HEK293 cells and *Drosophila*. (a and b)** Expression of ATP13A2 suppressed α-tubulin hyperacetylation in ATP13A2-deficient cells. ATP13A2-null HEK293 cells were transfected with either pcDNA3.1 (KO/Ctrl) or ATP13A2 (KO/ATP13A2 WT), followed by immunostaining with an anti–acetyl α-tubulin antibody (Ac-tub, green) and anti-FLAG (FLAG, to detect exogenous ATP13A2, red). Dashed lines indicate the cells expressing exogenous ATP13A2 (a). Quantitative analysis of acetyl α-tubulin intensity is shown (b). Bar, 6 µm. ****, P < 0.0001. KO/ATP13A2 WT: *n* = 51; KO/Ctrl: *n* = 46. **(c and d)** SIRT2 did not restore autophagic flux in ATP13A2-null HEK293 cells. Lysates of WT or ATP13A2-null HEK293 cells transfected with pcDNA3.1, HDAC6-FLAG, or SIRT2-V5 were immunodetected with anti-LC3B (LC3-I/LC3-II) antibody, anti-FLAG (FLAG) antibody, and anti-V5 (V5) antibody. α-Tubulin (α-tub) was detected to serve as a loading control (c). Quantitative analysis of LC3-II/α-tub is shown (d). ****, P < 0.0001, *n* = 3. **(e and f)** Regulation α-tubulin acetylation by *d*HDAC6 and *d*Sirt2 in flies. Fly head lysates were immunoblotted by an anti–α-tubulin (α-tub) antibody and an anti–acetyl α-tubulin (Ac-tub) antibody. Fly lines analyzed include control (Elav/+), elav-gal4 driven *d*HDAC6 RNAi (Elav>*d*HDAC6 RNAi), and *d*Sirt2 RNAi (Elav>*d*Sirt2 RNAi) lines (e). A quantitative analysis of acetylated α-tubulin/α-tubulin ratio is shown (f). **, P < 0.01; ***, P < 0.001, *n* = 3. *d*HDAC6 predominantly regulated α-tubulin acetylation in *Drosophila*. **(g)** HDAC6 predominantly regulated α-tubulin acetylation in follicle cells of flies. Fly follicle cells were probed for total α-tubulin (α-tub, red) and acetyl α-tubulin (Ac-tub, green). Fly lines analyzed included control Da-gal4 expressor (Da/+), *d*HDAC6 RNAi line, and *d*Sirt2 RNAi line. Representative images are shown. Bar, 10 µm. **(h and i)** Coimmunoprecipitation of ATP13A2 and HDAC6. Lysates of HEK293 cells expressing ATP13A2-FLAG (+) or control cells transfected with an empty pcDNA3.1 (–) plasmid were immunoprecipitated (IP) with anti-FLAG M2 antibody–conjugated agarose followed by immunoblot analysis (IB) with either an anti-HDAC6 antibody (h, top panel) or an anti-FLAG antibody (h, second panel from top). Input was analyzed by direct immunoblot analysis. β-Actin was detected to serve as a loading control for input (h, bottom panel). Note that overexpressed ATP13A2 coimmunoprecipitates with endogenous HDAC6. Inversely, lysates from HDAC6-null HEK293 cells and WT control cells expressing ATP13A2-FLAG were immunoprecipitated with an anti-HDAC6 antibody followed by immunoblot with either an anti-HDAC6 antibody (i, top panel) or an anti-FLAG antibody (i, second panel from top). Input was detected with either an anti-FLAG (FLAG) antibody or an anti-HDAC6 (HDAC6) antibody by direct immunoblot. β-Actin was detected to serve as a loading control for input (i, bottom panel). Note that endogenous HDAC6 coimmunoprecipitates with overexpressed ATP13A2. **(j and k)** LYS accumulation in ATP13A2-null HEK293 cells is reversed by expressing HDAC6. LYS in ATP13A2-null (KO/Ctrl) and WT control HEK293 cells were detected by immunostaining with an anti-LAMP1 antibody (green). Expression of HDAC6 (HDAC6 WT), but not the catalytic mutant (HDAC6 H611A), inhibited LYS accumulation in ATP13A2-null (KO) cells. Cell boundary is labeled by dashed lines (j). Quantification of LAMP1-positive structures was performed with ImageJ (k). Bar, 7.5 µm. ***, P < 0.001; ****, P < 0.0001. WT: *n* = 39, KO: *n* = 42, KO/HDAC6 WT: *n* = 36, KO/HDAC6 H611A: *n* = 47. **(l and m)** ATP13A2-regulated α-tubulin acetylation was inhibited by HDAC6 but not HDAC6 catalytic mutant in both HEK293 cells. α-Tubulin acetylation (Ac-tub, green) was detected in HEK293 cells. WT cells, ATP13A2-null cells (KO/Ctrl), ATP13A2-null cells expressing WT HDAC6 (KO/HDAC6 WT), and ATP13A2-null cells expressing HDAC6 catalytic inactive mutant H611A (KO/HDAC6 H611A) were analyzed. Expression of HDAC6 variants was detected with an anti-FLAG antibody (red). Cell boundary is indicated by dashed lines (l). Bar, 6 µm. Quantification of acetylated α-tubulin intensity per cell was performed with ImageJ software. Results from three independent experiments are shown (m). **, P < 0.01; ***, P < 0.001; ****, P < 0.0001. WT: *n* = 33, KO: *n* = 41, KO/HDAC6 WT: *n* = 47, KO/HDAC6 H611A: *n* = 39. **(n)** ATP13A2 regulates α-tubulin acetylation via HDAC6 in follicle cells of flies. Fly follicle cells were probed for total α-tubulin (α-tub, red), acetylated α-tubulin (Ac-tub, green). Fly lines analyzed include control Da-gal4 expressor (Da/+), *d*ATP13A2 RNAi line (Da>*d*ATP13A2 RNAi/Ctrl), and *d*ATP13A2 RNAi line expressing either *d*HDAC6 WT or *d*HDAC6 H664A. Bar, 10 µm. Note that detection of acetylated α-tubulin was markedly increased with dATP13A2 knockdown. The increased detection was inhibited by overexpressing HDAC6 WT but not the deacetylase mutant HDAC6 H664A.

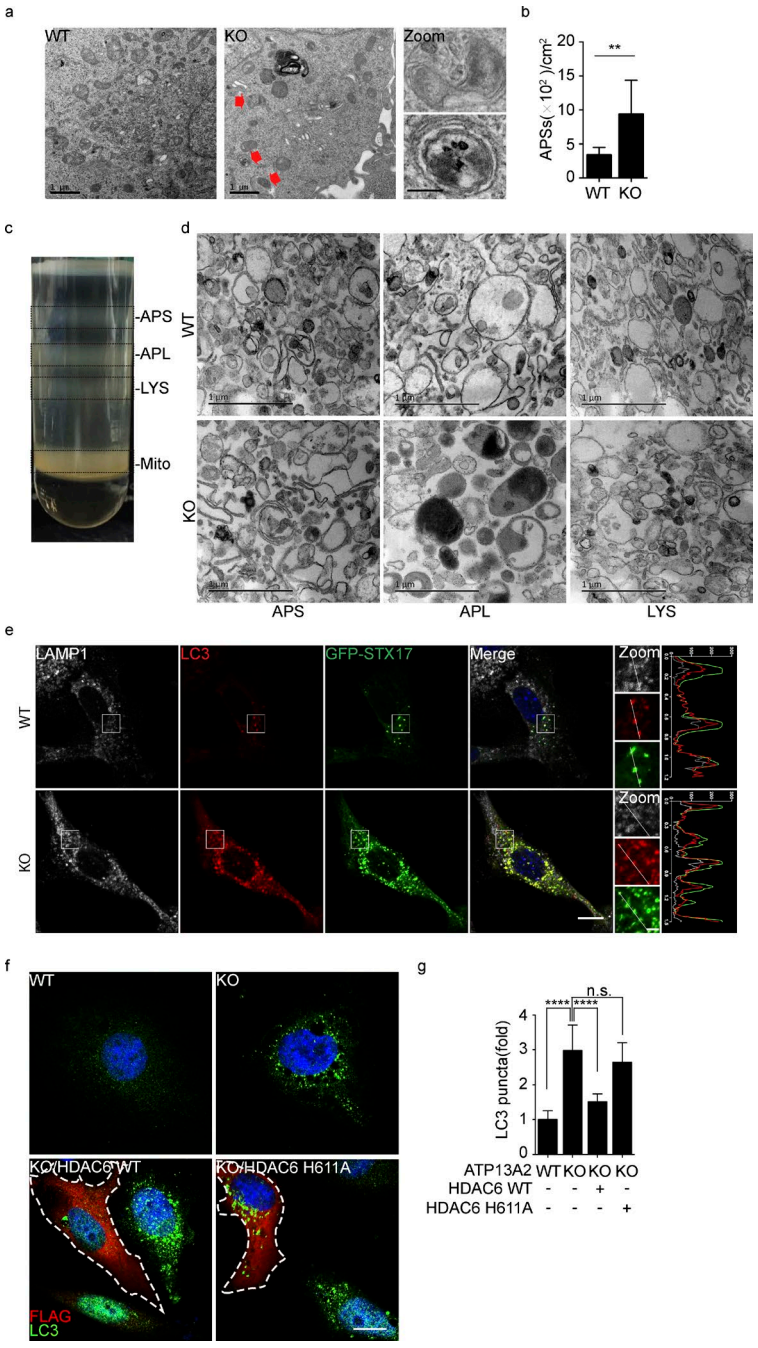

Figure S4. **Characterization of HDAC6 activity in ATP13A2-null cells and on LYS of ATP13A2-null mice. (a and b)** Accumulation of APSs in ATP13A2-null HEK293 cells. TEM analysis of control WT and ATP13A2-null (KO) HEK293 cells showed increased detection of APS (red arrows) in ATP13A2-null cells relative to their WT control cells (a, left two panels). Bar, 1 µm. Amplified images of APS from KO cells are shown in the two right panels (Zoom, bar, 0.2 µm) (b). Quantification of APS is shown in (b). **, P < 0.01. WT: *n* = 33, KO: *n* = 46. **(c and d)** Characterization of cell fractionation products from mouse livers. Subcellular fractionation was done with liver tissues of 5-mo-old mice. Fractions seen in a discontinuous Histodenz gradient (26%, 24%, 20%, and 15%) with protease inhibitors are shown (c). APS and LYS fraction at the interfaces of gradients were collected by syringe. The fractionation products were further characterized by TEM (d). Bar, 1 µm. APL, autophagolysosome; Mito, mitochondria. For TEM analysis, APS, autophagolysosome, and LYS fractions isolated from mouse livers were analyzed. Fractions were isolated from mouse livers of control WT ATP13A2 and ATP13A2 KO mice. **(e)** ATP13A2 KO does not affect syntaxin-17 distribution of APS and LYS. Control WT and ATP13A2-null (KO) MEF cells were transfected with a plasmid encoding GFP-STX17. Cells were immunodetected with antibodies against GFP (green), LC3B (red), and LAMP1 (gray). Bar, 7.5 µm. Selected regions (white boxes) are amplified to show the colocalization (Zoom, bar, 1.5 µm). Representative histograms of colocalization analysis are shown (right panel). Colocalization of STX17/LC3B/LAMP was clearly detected in control WT MEFs, whereas STX17 was mostly colocalized with LC3B in ATP13A2-null MEFs. The results suggest that ATP13A2 does not affect STX17 recruitment to APS. **(f and g)** HDAC6 promoted clearance of LC3 puncta in ATP13A2-null HeLa cells. ATP13A2-null HeLa cells were transfected with control plasmid pcDNA3.1 (KO) or plasmid encoding HDAC6 WT (KO/HDAC6 WT) or HDAC6 H611A (KO/HDAC6 H611A). Cells were coimmunostained with an anti-LC3B antibody (green). An anti-FLAG antibody (red) was used to detect expression of HDAC6 variants, Bar, 7.5 µm. Quantification of LC3 puncta is shown (f). ****, P < 0.0001. KO: *n* = 50, KO/HDAC6 WT: *n* = 49, KO/HDAC6 H611A: *n* = 39.

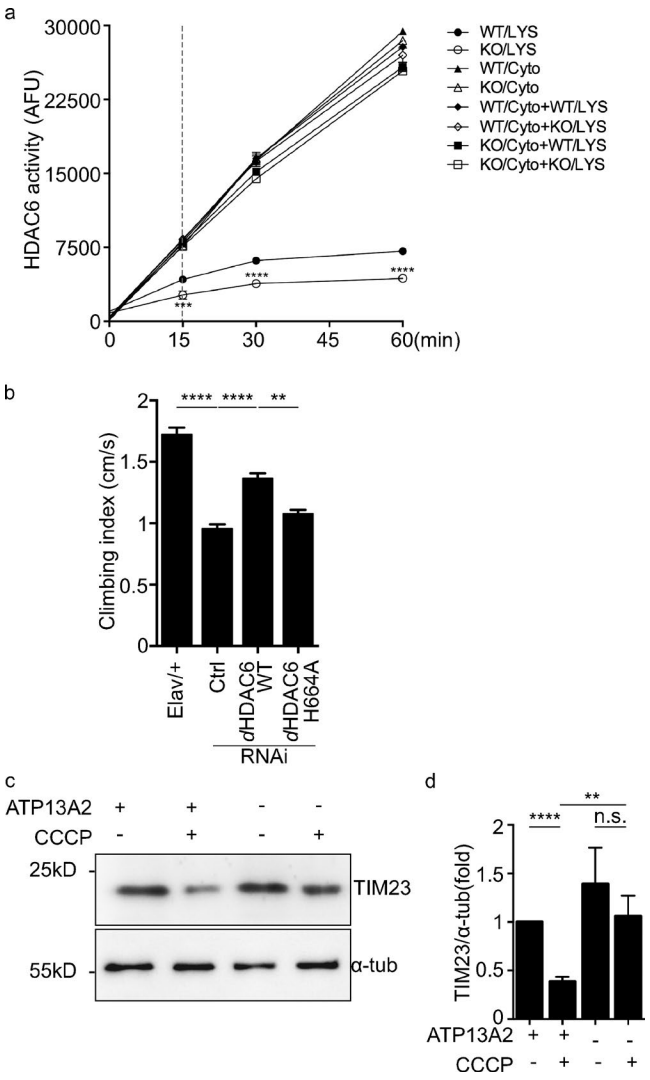

Figure S5. **Functional analysis of ATP13A2. deficiency. (a)** HDAC6 activity on LYS from WT mice was significantly higher than that from ATP13A2-null mice. LYS and cytosol (Cyto) were fractionated by using cell lysates from livers of either WT or ATP13A2-null (KO) mice. HDAC6 activity was determined with a commercial HDAC6 fluorimetric drug discovery kit. HDAC6 activities in LYS fractions from WT mouse livers (WT/LYS) or from ATP13A2-null mouse livers (KO/LYS), cytosol fractions from WT mouse livers (WT/Cyto) or ATP13A2-null mouse livers (KO/Cyto), a combination of both LYS fraction and cytosol fraction from WT mouse livers (WT/Cyto+WT/LYS), a combination of cytosol fraction from WT mouse livers and LYS fraction from ATP13A2-null mouse livers (WT/Cyto+KO/LYS), a combination of cytosol fraction ATP13A2-null mouse livers and LYS fraction from WT mouse livers (KO/Cyto+WT/LYS), and a combination of both cytosol fraction and LYS fraction from ATP13A2-null mouse livers (KO/Cyto+KO/LYS) were assayed. To test whether HDAC6 activity is LYS dependent, lysosomal LYS was added 15 min after activity assay initiation. The dashed line indicates the time point of adding LYS fraction into cytosol fraction. The HDAC6 activity was measured at 0, 15, 30, and 60 min. ***, $P < 0.001$; ****, $P < 0.0001$, $n = 3$. Note that HDAC6 activity was significantly higher in LYS fraction from WT mouse livers than in that from ATP13A2-null mouse livers. HDAC6 activity in cytosol fraction was markedly higher than that in LYS fractions. **(b)** Impaired climbing ability of *Drosophila* with *d*ATP13A2 knockdown. Flies with elav-driven *d*ATP13A2 RNAi coexpressing either WT *d*HDAC6 or catalytic inactive mutant *d*HDAC6 (H664A) were assayed for climbing ability. Flies expressing elav-gal4 alone (Elav/+) and *d*ATP13A2 RNAi alone (Ctrl) were included as controls. Climbing ability was assayed at fly age of 15 d. **, $P < 0.01$; ****, $P < 0.0001$. Elav/+: $n = 108$, RNAi/Ctrl: $n = 100$, RNAi/*d*HDAC6 WT: $n = 100$, RNAi/*d*HDAC6 H664A: $n = 103$. Knockdown of ATP13A2 in flies resulted in reduced climbing ability that was reversed by expressing WT HDAC6, but not the catalytic mutation of HDAC6. **(c and d)** Mitochondrial inner membrane protein TIM23 degradation was blocked in ATP13A2-null HEK293 cells. WT (ATP13A2, +) and ATP13A2-null (ATP13A2, –) HEK293 cells were treated with DMSO (CCCP, –) or CCCP (CCCP, +). Cell lysates were immunodetected by an anti-TIM23 (TIM23) antibody or an anti–α-tubulin (α-tub) antibody. Detection of α-tubulin served as a loading control (a). Quantitative analysis is shown (b). **, $P < 0.01$; ****, $P < 0.0001$, $n = 3$.